Microphysical estimation of the cloud vertical profile by a C-band polarimetric radar

R. BECHINI [(1)], E. DIETRICH, R. FABBO [(1)], M. BERTATO [(1)]

(1) *Weather Radar Operations Center, ERSA/CSA Friuli - Venezia Giulia, Fax: +39-0431-88074 – web page: http://www.radar.csa.fvg.it*

ABSTRACT

Most recent approaches to multisensor rainfall estimation require a characterisation of the microphysical tridimensional structure of the cloud. This can be usefully done by a ground based polarimetric radar.

The use of polarimetric radar measurements, in particular the differential reflectivity, makes it possible to distinguish in most cases between liquid and ice phase of meteorological particles. Adding the information given by the horizontal reflectivity Z_H, it is possible to identify different hydrometeors in the same thermodynamic phase. Anyway, in some cases the same couple of Z_H, Z_{DR} values can not univocally be associated to a single hydrometeor type. In such cases the recognition of the melting layer, by means of the gradient of Z_{DR} along the beam and the temperature profile of the nearest radiosounding, can help in distinguish between the different particles, even if a certain degree of uncertainty still remains.

In this paper an algorithm based on measured values of Z_H and Z_{DR} is illustrated. The tridimensional space Z_H, Z_{DR}, h (height of the radar cell) has been opportunely partitioned, so that each point of this space corresponds to a distinct hydrometeor type or mixture. For every radar cell it is then possible to identify the particle (or mixture) associated and calculate the corresponding *LWC*. Finally the microphysical vertical profile above every point of the radar domain can be built.

1 INTRODUCTION

The need for microphysical characterisation of the cloud vertical profile by the satellite precipitation retrieval algorithms and in particular the combined radar-model-SSM/I approach [1] was the main reason to further develop the ongoing research on particle identification at the meteorological radar centre of Fossalon di Grado.

Actually a polarimetric radar is the most suitable instrument to operationally identify the hydrometeor type and calculate the associated *LWC* over a wide area.

The use of differential reflectivity (Z_{DR}) measurements makes it possible to distinguish between liquid and ice phase of meteorological particles. Falling raindrops are not spherical but have an oblate shape with, in still air, minor axis vertical [2], moreover axial ratio only depend on the D_e diameter of the equivalent sphere [3]. Differently, the shape of ice particles (such as ice crystals, aggregates, snow, graupel, hail) does not underlie a simple relation like that for liquid drops.

The common intent of the studies devoted to the microphysical interpretation of the radar signal is to relate the measured quantities (in the case of the GPM-500C radar of Fossalon [4], the reflectivity Z_H and the differential reflectivity Z_{DR}) to the properties of hydrometeors [5].

A relevant difficulty arises when the backscattered radar echo is low. In fact, for reflectivity values below 20-25 dBZ the water droplets are nearly spherical, consequently the typically very small values assumed by Z_{DR} could fit equally well to water particles as well as to randomly oriented ice crystals or aggregates.

As it will be shown, this problem can be usefully overcome in the case of stratiform precipitation systems (as those induced by Atlantic fronts associated with deep trough and Southerly flow over the Alpine region), by the use of the gradient of Z_{DR} along the radar beam, in order to estimate the height and depth of the melting layer.

2 PARTICLE IDENTIFICATION

Several authors [5], [6], [7] have made attempts to synthesise the results of models, observations and experience of various investigators, in order to produce a simple tool for particle identification. An example is given in Table 1, where a summary listing of the particle type versus range values for the polarimetric measurands [5] is partially reproduced (only Z_H and Z_{DR} are considered here).

From this table it appears clearly that different pairs of measurands (Z_H, Z_{DR}) can fit equally well to distinct hydrometeor types, namely the radar polarimetric measurands do not lead to univocally identify the particle type.

A possible solution to limit the problem of the overlapping arises from splitting up vertically the atmosphere and producing different masks like Table 1, one for each layer.

Exploiting the well known phenomena of the *bright band* it is possible to split the portion of the atmosphere seen by the radar in at least four layers: below the melting layer, lower melting layer, upper melting layer and above the melting layer.

	Z_H (dBZ)	Z_{DR} (dB)
Drizzle	< 25	0
Rain	25 to 60	0.5 to 4
Snow, dry, low density	< 35	0 to 0.5
Crystal, dry, high density	< 25	0 to 5
Snow, wet melting	< 45	0 to 3
Graupel, dry	40 to 50	-0.5 to 1
Graupel, wet	40 to 55	-0.5 to 3
Hail, small (<2 cm) wet	50 to 60	-0.5 to 0.5
Hail, large (>2 cm) wet	55 to 70	< -0.5
Rain & Hail	50 to 70	-1 to 1

Table 1. Values of Z_H and Z_{DR} for various hydrometeor types (adapted from Doviak [5]).

2.1 Assessment of the melting layer height and depth

The *bright band* is a very common feature in stratiform precipitation. It is due to the melt of ice particles below the freezing level. The abrubt change in the dielectric factor (for the ice $|K|^2_i$=0.176, while for water $|K|^2_w$=0.93) causes the reflectivity to assume higher values within the melting layer.

As the snowflakes melt they become increasingly oblate, leading to a consequent increase in the differential reflectivity values too. Following this change of shape, the particles, upon completion of melting, collapse to raindrops of sizes much smaller than those of snowflakes, but with widely different fall speeds, all of which are much larger than those of the original flakes [8]. This causes both the reflectivity and differential reflectivity to decrease below the melting layer (Fig. 1). In some cases drop break-up and shedding can occur in the lower melting layer.

Even if the peak of Z_{DR} frequently lies about 200 m below the Z_H peak [9], the gradient (with gradient is intended here the first degree derivative along the beam) of the two variables below the peak becomes zero nearly at the same height, correspondingly to the end of melt (Fig. 1).

The first degree derivative along the beam is considered, instead of the vertical gradient, because to calculate the vertical gradient a set of quasi-continuous elevation would be needed (not feasible within a reasonable acquistition time). Except for very low elevation angles, the variability along the beam in stratiform clouds at the height of the melting layer can reasonably

be mainly attributed to the vertical component of the gradient rather than to the horizontal (Fig. 2).

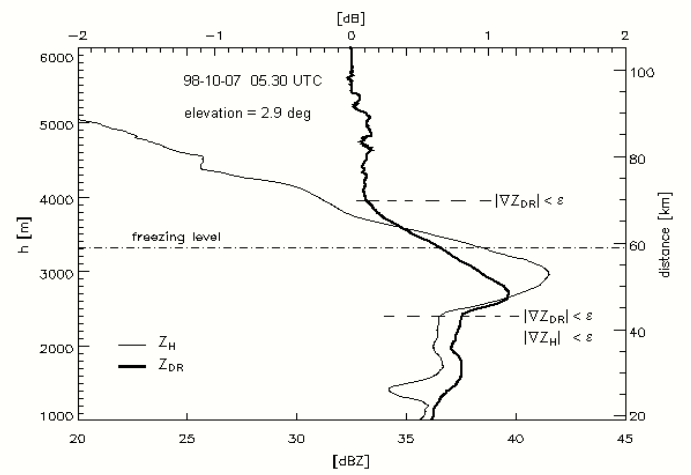

Figure 1. Reflectivity Z_H and differential reflectivity Z_{DR} averaged over azimuth for a 2.9 deg radar elevation scan. The left vertical axis gives the relative height of the radar cell. The two horizontal solid lines show where the absolute value of the first degree derivatives are nearly zero, below (Z_{DR} and Z_H) and above (only Z_{DR}) the peaks.

Z_{DR} seems more appropriate than Z_H in identifying the upper melting layer boundary, because while Z_H often decreases monotonically with height, the gradient of Z_{DR} turn again to near zero values, where the cloud is mainly composed by ice particles (Fig. 1).

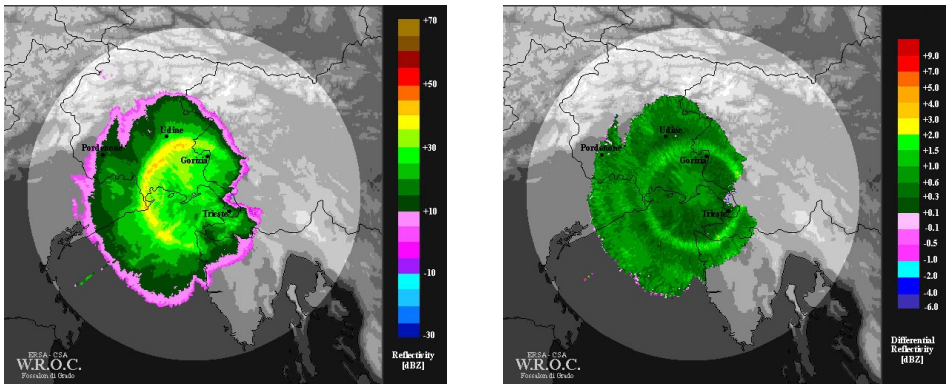

Figure 2. 5.5 deg PPI, September 20th 1999 15.00 UTC. A 2.25 km length median filter is applied along the beam in order to smooth the data over measurements errors. The spot light indicates the radar range (110 km). Clearly visible is the bright band between 30 and 40 km range on Z_H (left) and Z_{DR} (right), due to the melt of ice particles below the freezing level.

Moreover, the *bright band* on Z_{DR} is detectable even when the backscattered radiation is weak (due to wettening of preferentially horizontally oriented ice crystals [10]), while in those cases the *bright band* on Z_H is not so noticeable (Fig. 2).

For these reasons the gradient of Z_{DR} is used here to identify the Melting Layer (since now ML). This is done through a rough analysis of the gradient of Z_{DR} as shown in Fig. 3. The identification of the ML boundaries is driven by the nearest radiosounding 0° C and 5° C levels [11], in order to avoid eventual gross misinterpretations of the Z_{DR} gradient. This is of relevant importance at low elevation angles, where the analysis of the Z_{DR} gradient alone doesn't guarantee a correct ML identification, due both to the reduced vertical component of the gradient and to the beam-spreading effect.

The medium ML level drawn in Fig. 3 corresponds to the peak of Z_{DR} and it is physically related to the maximum particle oblateness, namely below that level most of the particles completely melt, collapse into smaller raindrops and may undergo drop break-up.

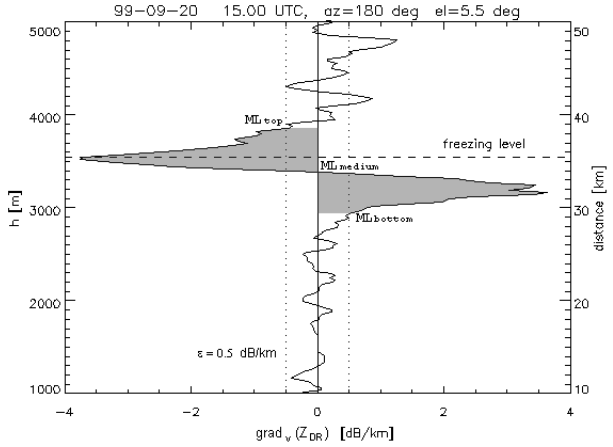

Figure 3. Identification of the ML boundaries by means of the vertical projection of the Z_{DR} gradient. The size of the shaded area (integral of $|\text{grad}_v(Z_{DR})|$ between ML_{bottom} and ML_{top}) is a measure of the Z_{DR} gap due to the melting layer.

2.2 Particle identification masks for different atmospheric layers

With this four layer partition of the atmosphere (below the ML, lower ML, upper ML and above the ML) it is possible to produce a set of more specific particle identification masks like that shown in Table 1.

The fundamental radar distinction between liquid particles and non-liquid particles (ice or mixed phase) can be usefully explained producing a number of synthetic drop size gamma distributions:

$$n(D) = n_0 D^m e^{-\Lambda D} \tag{1}$$

where D is the drop diameter. Integrating between D_{min}=0.1 mm and varying the three coefficients and the upper integral limit D_{max} within the following values [12]:

$$30 \le n_0 \le 30000 \qquad (\text{mm}^{-1}\text{m}^{-3})$$
$$-2.0 \le m \le +3.0$$
$$1.0 \le \Lambda \le 4.5 \qquad (\text{mm}^{-1})$$
$$4.0 \le D_{max} \le 6.0 \qquad (\text{mm})$$

it is possible to calculate the theoretical Z_H and Z_{DR} for liquid drops [12]. In Fig. 4 the scatter plot of the Z_H and Z_{DR} values obtained from nearly 3500 distributions is shown.

This theoretical result, together with various experimental outcomes from inter-comparisons between radar data and in situ measurements [5] [6] [10], led to the particle identification masks in Fig. 5. Those masks, based on the ML recognition described in section 2.1 are considered valid only for stratiform precipitation (values of Z_H above 50 dBZ, associated with hail possibility, are left on the masks to cover the entire Z_H range, but are not observed in stratiform rain).

The partitions of the Z_H, Z_{DR} space in Fig. 5 shows that a certain degree of overlapping is still present, especially in the upper ML region. In particular it is difficult to distinguish between droplets, crystals and dry snow for low values of Z_H and nearly zero Z_{DR}. It would be possible (not dealt in this paper), on the other hand, to give the percentages of the total liquid water content for the hydrometeors R (rain/liquid droplets) and WS (wet snow) in the ML. This could be done simply by assuming a linear decrease with height within the ML of the R liquid water content percentage or adopting a more sophisticated ML model.

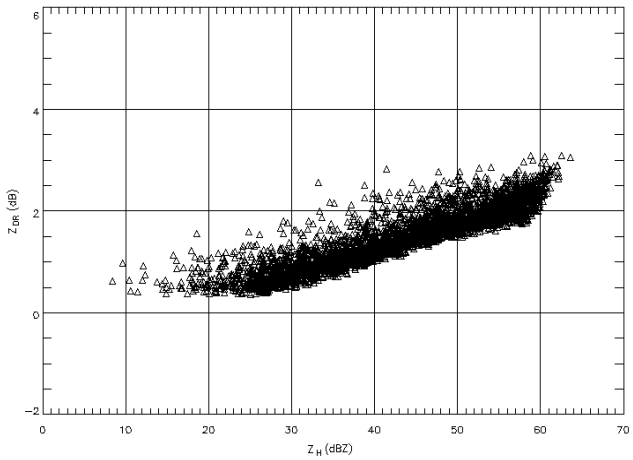

Figure 4. Scatter plot of Z_H and Z_{DR} computed on the basis of nearly 3500 drop size gamma distributions (eq. (1)).

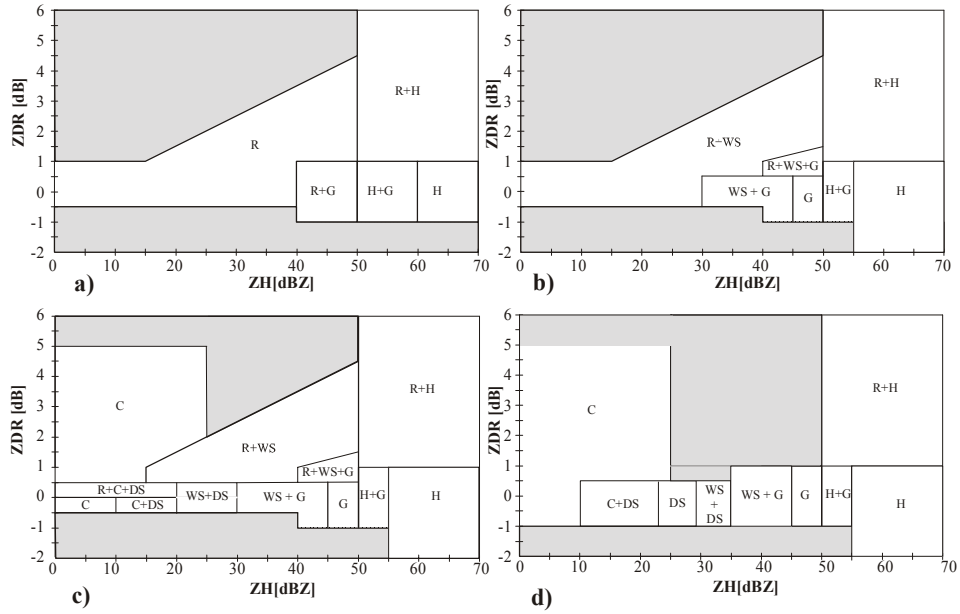

Figure 5. Particle identification masks for below the ML (a), lower ML (b), upper ML (c) and above the ML (d). R: rain/liquid droplets, WS: wet snow, DS: dry snow, G: graupel, H: hail, C: crystals. The sign + point out the possible coexistence of several hydrometeors in the same radar volume.

3 LIQUID WATER CONTENT ESTIMATION

Estimation of the *LWC* (*IWC*) is a matter of applying several appropriate relations, once the particle type has been identified. To obtain reliable estimates of mass content from the measured radar reflectivity, the particle must be spherical or treated as equivalent spheres with diameters D that are small in comparison to the radar wavelenght.

Moreover, the thermodynamic phase of the scatterers must be known in order to derive Z_H, because the reflectivity is a function of the dielectric factor $|K|^2$, which in turn is a function of the particle phase. The standard radar systems (like the GPM-500C) determine the water equivalent radar reflectivity ($Z_{H(e)}$), namely the reflectivity of the target in the hypothesis that the scatterers are spherical water droplets. The conversion factor to obtain the ice equivalent radar reflectivity ($Z_{H(i)}$) is given by $|K^2_w|/|K^2_i|$ (where $|K|^2_w=0.93$ and $|K|^2_i=0.176$ for $\lambda>3$ cm), that is:

$$Z_{H(i)} = 5.28 Z_{H(e)}$$

where $Z_{H(e)}$ and $Z_{H(i)}$ are in mm^6m^{-3}. In decibels, the corresponding difference is 7.2 dB. The relations used to calculate the particle *LWC* (*IWC*) are exponential functions of $Z_{H(x)}$:

$$LWC = AZ_{H(x)}^{B} \quad (2)$$

where $x=i$ for DS (dry snow), while $x=w$ for all the other particles, $Z_{H(x)}$ is in mm^6m^{-3} and LWC in gm^{-3} (note that the relation for the ice crystals IWC is expressed as a function of $Z_{H(e)}$).

Given in Table 2 are the coefficients A and B used for the different hydrometeor types.

Particle	x	A	B	Reference
R	w	0.0017570	0.667	Gorgucci *et al.* [13]*
WS	w	0.0024379	0.560	Holler (1995) [14]
DS	i	0.0030000	0.605	Herzegh and Hobbs [15]
C	w	0.0320000	0.505	Heimsfield (1977) [16]
G	w	0.0024379	0.560	Holler (1995) [14]
H	w	0.0001867	0.666	Holler (1995) [14]

Table 2. List of the coefficients A and B used in eq. (2) for the LWC (IWC) calculation; the second column point out whether the water (w) or ice (i) equivalent reflectivity is used for LWC estimation. * for Z_H-$Rain$ relation, then LWC-$Rain$ based on [11].

The coefficients in Table 2 have been chose within a variety of similar LWC-Z_H relations, as the more suitable to the kind of meteorological system treated in this study (mid-latitudes stratiform precipitation). However, especially for IWC determination, the extreme variability from day to day and from cloud to cloud reflects in quite high uncertainty.

For the purely liquid phase (hydrometeor R) it is possible to have an indirect experimental estimation of the standard error in the Friuli region, through a rain gage – radar reflectivity inter-comparison. Fig. 6 shows a scatter plot of the rain gage (9 stations up to 75 km from the radar site) one hour cumulated precipitation versus the radar reflectivity based estimate.

Given the analogous theoretical assumptions at the roots of the Z_H-$Rain$ and Z_H -LWC relations, the error found for rainfall estimation is assumed here for the LWC estimation too (-40%, +65%).

The lack of experimental results regarding the LWC estimation in the melting layer induced who writes to assume for wet snow and graupel LWC estimates the error introduced by an hypothetical variation of the dielectric factor from the value corresponding to pure water to that of pure ice. That means an error on the LWC estimate of (-60%, +130%).

The results obtained by Atlas [17] are used in this paper in order to establish the error range for dry snow and crystals. Atlas [17] found that the scatter in the Z_H-logLWC distribution on 5104 samples collected during the FIRE I experiment (Wisconsin, 1986), decreases significantly with increasing Z_H. This is attributed to the fact that near largest reflectivities there is a narrow range of the particle median volume diameter. In rain-type acquisition mode the lower signal detectable by the GPM-500C is between –10 and 0 dBZ. Therefore, as the error range inferred from Atlas [17] in this reflectivity range is about 0.5 on

log*LWC* (*LWC* in g/m^3), it reasonable assuming an upper limit to the percent error range of about (-70%, +215%). Moreover, it should be kept in mind that a sizeable fraction of radiatively significant cloud is missed by a C-band radar, since ice crystals samples with corresponding theoretical reflectivity up to –50 dBZ have been observed in cirrus clouds [17].

No attempt at the moment is made to quantify the error on hail estimates.

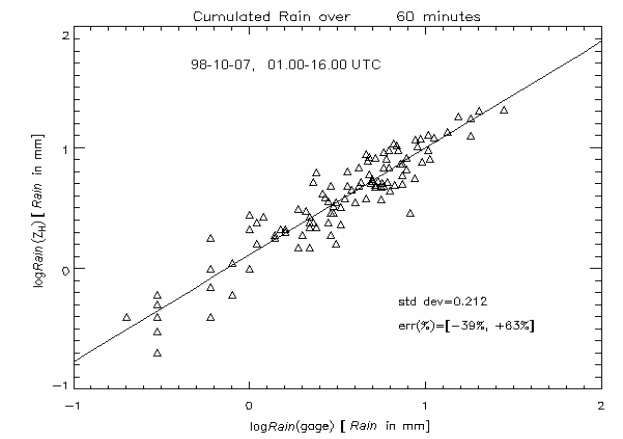

Figure 6. Scatter plot between rainfall accumulation at ERSA/CSA stations and the corresponding rainfall accumulation obtained from the GPM-500C Fossalon radar. Standard deviation of the log*Rain(gage)*-log*Rain*(Z_H) distribution and the percent error on *Rain* estimate are shown.

4 EXAMPLES OF MICROPHYSICAL PROFILES ESTIMATION

In this section a few examples of the cloud microphysical vertical profile estimation are given, making use of two flood-like events, mainly characterised by long lasting stratiform rain.

4.1 October 7th, 1998

On October 6, a cold drop detached from a trough extending over the Western Mediterranean Sea (cut-off), leading to the formation of a wide depression area over the Central and Western Mediterranean Sea. The depression and the associated cold front, moving from South-West to North-East, determined very moist Scirocco winds from sea level to higher altitudes, producing intense and widespread rain during the night of October 6-7 and the following day.

During this event the radar was operating in a rain-type acquisition mode, consisting of five low elevations (0.5, 1.0, 1.5, 1.9, 2.9), a 125 m cell size and a time sampling of 10 minutes.

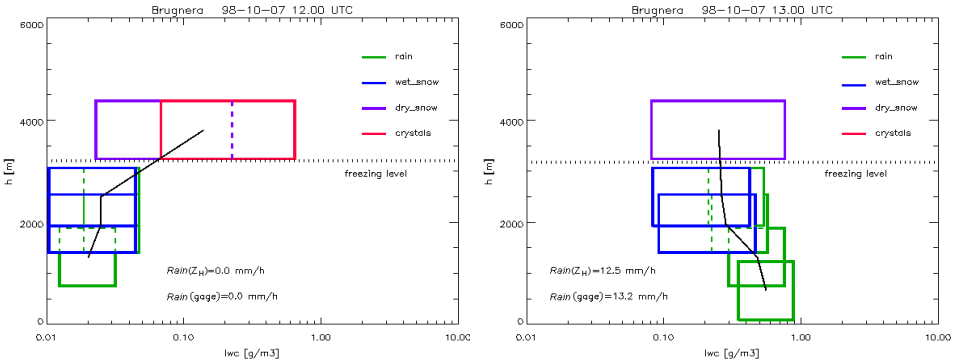

Figure 7. Microphysical vertical profile estimation above the Brugnera ERSA/CSA station, located 75.3 km W-NW from the radar site, obtained from a five elevations (0.5, 1.0, 1.5, 1.9, 2.9) volume scan. The width of the rectangles corresponds to the assumed measurement error, while the height gives the radar beam dimension at the station distance. The black solid line represents an interpolation of the mean (when more than one hydrometeor type is present) *LWC*. The gage extrapolated *Rain* intensity and the radar estimate are also shown.

In Fig. 7 two microphysical vertical profiles above one of the ERSA/CSA stations are shown. Although the quite large errors prevent from detailed physical interpretation, it is worth noting that the onset of precipitation at surface level (as testified by the station gage) is associated with a general increase of the *LWC* values along the portion of the troposphere seen by the radar. Moreover a shift of the *LWC* towards the lower levels seems to have occurred in the elapsed time between the two radar volume scans the images refer to.

4.2 September 20th, 1999

A deep trough interested Northern Italy starting the night between September 19th and 20th, giving large precipitation amounts over Piedmont and Lombardia. Later in the day the front interested mainly the North-East. Mid and upper level intense South-Westerly flow and lower level South-Easterly winds set up the ideal condition for heavy precipitation on the South flank of Carnian Alps. Precipitation amounts up to 350 mm in 24 hours in the pre-Alpine Western Friuli region where registered.

During this event a new acquisition mode has been used. The adoption of a larger cell size (250 m instead of 125 m) allowed to enrich the set of elevations (four higher elevations have been added) without change the 10 minutes time sampling. A more detailed tridimensional description of the event is therefore obtained. Fig. 8 (left) shows an application of the particle identification algorithm (section 2.2) on a 5.5 deg PPI, where the highly stratified structure of the system is noteworthy. The microphysical vertical profile above the ERSA/CSA Cervignano station is also shown (Fig. 8, right).

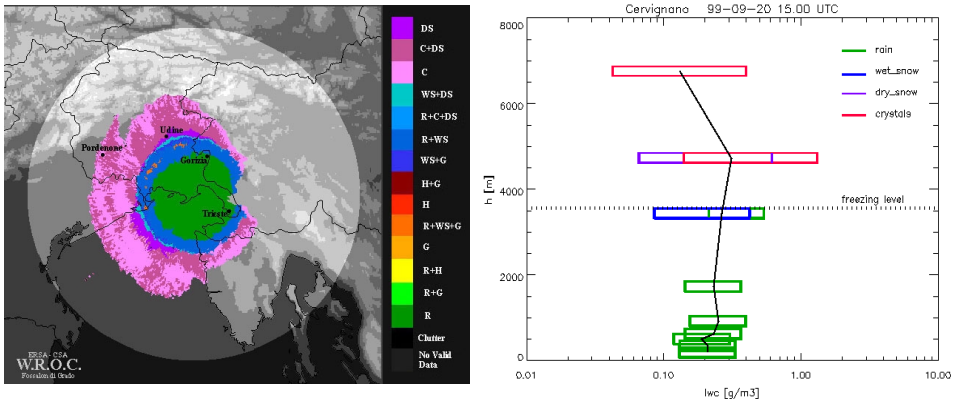

Figure 8. Particle identification 5.5 deg PPI, September 20th 1999 15.00 UTC (left). Microphysical vertical profile estimation above the Cervignano ERSA/CSA station, located 17.5 km N-NW from the radar site (right). Same as Fig. 7, except that a nine elevations (0.5, 1.0, 1.5, 1.9, 2.9, 5.5, 10.9, 14.9, 21.9) volume scan has been used.

5 CONCLUSIONS

The method presented in this paper has been thought and developed to respond to the need of a reliable selection criteria within a cloud database of simulated profiles. The radar-model-SSM/I approach developed by Dietrich *et al.* [1] uses the radar estimates to extract the more similar simulated profiles from a cloud database.

This approach showed good potentiality in improving the accuracy of SSM/I rainfall rate estimations [1]. At the moment the microphysical information derived from radar measurements (especially the ice phase) is subjected to quite large uncertainty, due both to the natural variability of particle size distribution and to the lack of *in situ* measurements. For this reason the radar estimates are not used straight in the combined approach, but serve to drive the selection of simulated profiles.

More *in situ* measurements and better understanding of the melting layer and ice phase microphysiscs are needed in order to improve the upper levels *LWC* estimate from radar measurements.

REFERENCES

[1] Dietrich S., R. Bechini, E. D'Acunzo, S. Di Michele, R. Fabbo, A. Mugnai, S. Natali, F. Porcu', F. Prodi, L. Roberti, and A. Tassa: Multisensor analysis of Friuli event (October 5-7, 1998). Proc. from 6th Specialist Meeting on Microwave Radiometry and Remote Sensing of the Environment (MICRORAD) Firenze, Italy - March 16-18, 1999. In Press.

[2] Sauvageot, H.: Rainfall Measurement by Radar: a Review. Atmospheric Research, 35, 27-54.(1994)

[3] Green, A.W.: An Approximation for the Shape of Large Raindrops. J. Appl. Meteorol.14, 1578-1583.(1975)

[4] Dietrich, E.: GPM-500C/F - A Polarimetric Doppler Radar for Research, Hail Detection, General Monitoring. ERSA Friuli Venezia Giulia, Gorizia. (1994)

[5] Doviak, R.J., D.S. Zrnic: Doppler Radar and Weather Observations. Academic Press, inc. (1993)

[6] Holler, H., V.N. Bringi, J. Hubbert, and P.F. Meischner: Particle discrimination in hailstorms. 26th Conf. on Radar Meteorology, Norman, OK, , Amer. Meteor. Soc., 594-595. .(1993)

[7] Brandes, E.A., J. Vivekanandan, J.D. Tuttle, C.J. Kessinger: Sensing thunderstorm microphysics with multiparameter radar: application for aviation. Preprints, 5th Conf. On Aviation Wea. Systems, 2-6 August, Vienna, VA, 98-102.(1993)

[8] Steiner, M. and A. Waldvogel: The bright band and its influence on microphysics. 24th Conf. on Radar Meteorology, Tallahassee, Florida, Amer. Meteor. Soc., 5-8.(1989).

[9] Moninger, W.R., V.N. Bringi, T.R. Detman, J.R. Jordan, T.A. Seliga, K. Aydin: Melting layer observations during MAYPOL. 22nd Conf. on Radar Meteorology, Zurich, Switzerland, Amer. Meteor. Soc., 364-369.(1984).

[10] Meischner, P., V.N. Bringi, M. Hagen, H. Holler: Multiparameter radar characterization of a melting layer compared within situ measurements. 25th Conf. on Radar Meteorology, Paris, France, Amer. Meteor. Soc., 721-724.(1991).

[11] Pruppacher, H.R. and J.D. Klett: Microphysics of Clouds and Precipitation. Kluwer Academic Publisher. (1997).

[12] Sachidananda, M., D.S. Zrnic: Rain Rate Estimates from Differential Polarization Measurements. *J. Atmos. Oceanic. Technol*., 4, 588-598.(1987).

[13] Gorgucci, E, G. Scarchilli and V. Chandrasekar: A robust estimator of rainfall rate using differential reflectivity. J. Atmos. Ocean. Technol., 11586.(1994).

[14] Holler, H.: Radar-derived mass-concentrations of hydrometeors for cloud model retrivals. Preprints, 27th Conf. on Radar Meteorology, Vail, CO, Amer. Meteor. Soc., 453-454.(1995).

[15] Herzegh, P.H. and P.V. Hobbs: The mesoscale and microscale strucure and organization of clouds and precipitation in mid-latitude cyclones. II: Warm frontal clouds. J. Atmos. Sci., 37, 597-611.(1980).

[16] Heymsfield, A. J.: Precipitation development in stratiform ice clouds: A microphysical and dynamical study. J. Atmos. Sci., 34, 367-381.(1977).

[17] Atlas, D., S.Y. Matrosov, A.J. Heymsfield, M.D. Chou and D.B. Wolff: Radar and radiation properties of ice clouds. J. Appl. Meteorol., 34, 2329-2345.(1995).